Supplementary Information: Strong coupling of two individually controlled atoms via a nanophotonic cavity

Polnop Samutpraphoot,[1, *] Tamara Đorđević,[1, *] Paloma L. Ocola,[1, *]
Hannes Bernien,[2] Crystal Senko,[3, 4] Vladan Vuletić,[5] and Mikhail D. Lukin[1, †]

[1]*Department of Physics, Harvard University, Cambridge, Massachusetts 02138, USA*
[2]*Pritzker School of Molecular Engineering, University of Chicago, Chicago, IL 60637, USA*
[3]*Department of Physics and Astronomy, University of Waterloo, Waterloo, N2L 3R1, Canada*
[4]*Institute for Quantum Computing, University of Waterloo, Waterloo, N2L 3R1, Canada*
[5]*Department of Physics and Research Laboratory of Electronics,*
Massachusetts Institute of Technology, Cambridge, MA 02139, USA

I. APPARATUS

The apparatus consists of a confocal microscope that images a photonic crystal (PC) installed in the glass cell of the vacuum chamber (Fig. S1). The microscope objective [Mitutoyo G Plan Apo 50X] is used for focusing optical tweezers (beam waist $w_0 \sim 900$ nm) and for fluorescence imaging of single atoms. The two tweezers are generated by combining two optical paths on a 50:50 non-polarizing beam splitter at the focus of a $4f$-microscope configuration. Each path also has two dichroic mirrors, to combine the trap light (815 nm) with individual repumping light (795 nm) and to separate the collected fluorescence light (780 nm).
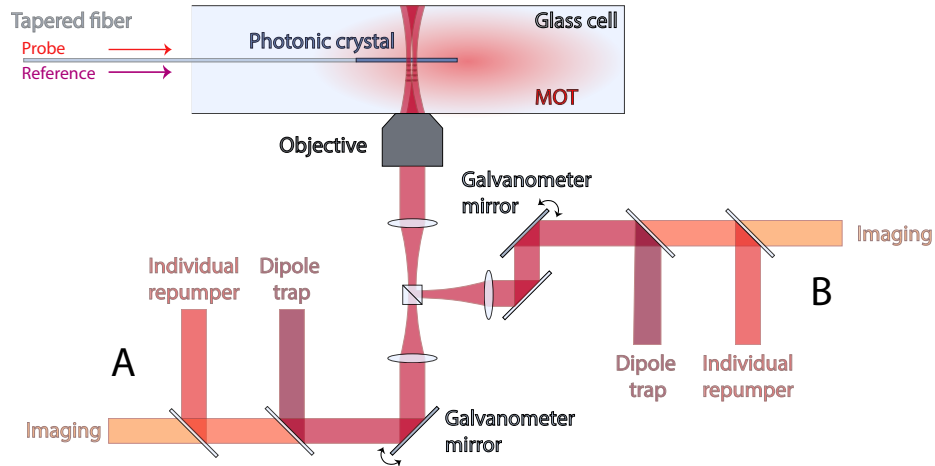

FIG. S1: Schematic of experimental setup (not to scale) detailing how the trap paths are combined and focused by the objective onto the PC. Resonant light is sent through the tapered fiber to the PC to probe the atom-cavity response, along with far-detuned light for cavity stabilization, which is continuously monitored in reflection.

The ultra-high vacuum (UHV) system consists of a glass cell mounted to a compact vacuum cube [Kimball Physics MCF450-SphSq-E2C4] and a combination of a non-evaporable getter and an ion pump [NEXTorr D300-5]. The entire system is mounted on a translation stage that can be retracted for device exchange without disturbing the optical paths around the chamber. The small and moveable vacuum system allows for speed-up of typically extensive

———————
*These authors contributed equally to this work
†lukin@physics.harvard.edu

procedures such as device replacement and pumping to UHV, which in our system can take less than one week in total. The PC is suspended at the tip of a tapered fiber [1], which is mounted on a rod assembly and led to the outside of the vacuum through a fiber feedthrough [2]. The probe light is sent to the cavity through a beam-sampler and coupled into the fiber, where the reflection is collected through the transmission port and onto a single-photon counter [PerkinElmer SPCM-AQR-16-FC]. The reference light for cavity stabilization is combined with the probe on a dichroic before coupling into the fiber and is monitored in reflection with a high-bandwidth avalanche photodiode [Menlo Systems APD210].

II. PHOTONIC CRYSTAL CAVITIES

Design and fabrication

The design of the cavity follows that in [3, 4]. The cavity used in this work is designed to operate near the critical coupling regime ($\kappa_{wg} \approx \kappa_{sc}$) for a minimal total loss rate $\kappa = \kappa_{wg} + \kappa_{sc}$. Since κ_{sc} is limited by fabrication imperfections, we decrease κ_{wg} by controlling the loss from the first Bragg mirror with the number of holes that define it, as shown in Fig. S2. To reach the critical coupling regime, κ_{wg} is tuned to be comparable to the loss from the cavity into free space κ_{sc} which has typical values of several gigahertz. The device used in this work has $\kappa_{wg} = 2\pi \times 0.86$ GHz and $\kappa_{sc} = 2\pi \times 2.77$ GHz.
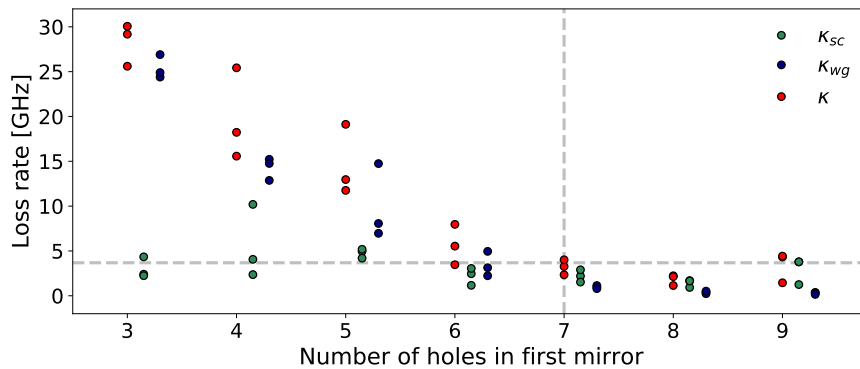

FIG. S2: Modifying the first mirror loss with the number of holes in the first mirror of the PC and comparing the loss rates for several devices with each hole number. Grey lines are drawn to indicate the number of holes chosen for the current cavity and its total loss of $\kappa = 2\pi \times 3.68$ GHz.

The fabrication process begins with a 200 nm layer of silicon nitride (bulk index of refraction = 2.02) on a silicon wafer [Silicon Valley Microelectonics, Inc.]. A pattern of 500 devices is created by exposing a layer of resist [ZEP520A] on the wafer to a scanning electron beam [Elionix F125]. The pattern is then transferred to the silicon nitride layer using reactive ion etching. The silicon underneath is removed in a wet etch process with KOH. At the end of the process, we deposit an absorptive material (amorphous silicon) onto the disk-shaped heater pad region for thermal tuning of the resonance.

Frequency stabilization of the cavity

The resonance of the fundamental mode of the nanophotonic cavity sits near the $5S_{1/2} \rightarrow 5P_{3/2}$ transition at 780 nm, but there exist higher-order modes at longer wavelengths as shown in Fig. S3a. For the device used in this work, the second-order mode has a resonance near 810 nm, which is off-resonant for the atoms, and has a linewidth of $2\pi \times 17$ GHz. A laser pointed at the heater pad region heats up the device and changes the index of refraction, tuning the resonances by the same increment, as shown in Fig. S3b. The bandwidth of the feedback loop is limited by this thermal tuning process at several milliseconds.

We stabilize the cavity monitoring the second-order mode and feeding back to the tuning laser power. The error signal is generated by modulating the phase of the reference light at 810 nm continuously sent to the cavity at 1 GHz.

The reflected signal from the monitoring avalanche photodiode is demodulated at the same frequency, creating a low-modulation Pound-Drever-Hall error signal (Fig. S3c) [6]. In the experimental sequence described in the next section, the cavity resonance must be tuned in and out of resonance during each trial for different probe pulses. We achieve this by jumping the setpoint and waiting for several milliseconds for the cavity to settle before probing. We have observed no degradation in the quality factor after inserting our current device within the vacuum system and continuously tuning and stabilizing its resonance for over one year.
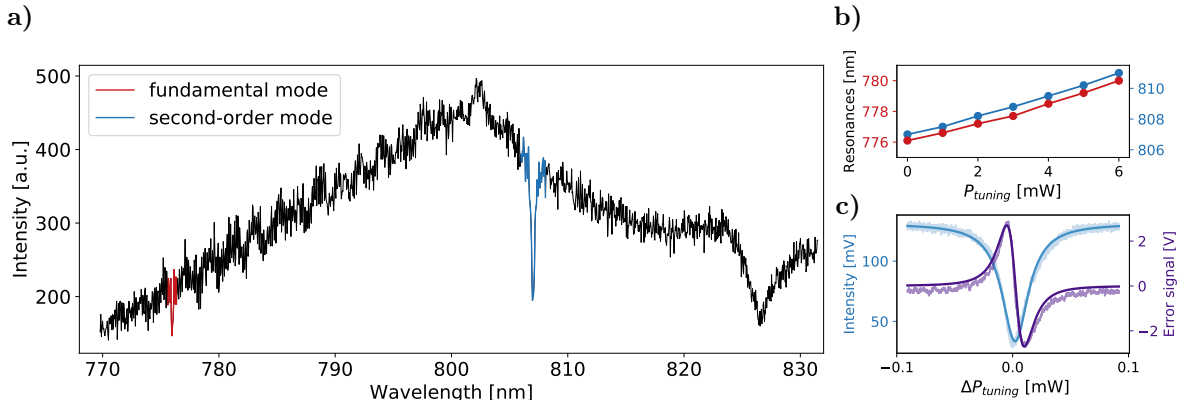

FIG. S3: **a)** Different resonances of the PC cavity observed by sending broadband light and collecting in reflection on a spectrometer. **b)** Simultaneous tuning of the first (red) and second (blue) order resonant wavelengths by increasing the tuning laser power incident on the heater pad. **c)** A reflection spectrum of the second order resonance (blue) and the PDH signal from the spectrum (purple) obtained from sweeping the tuning laser power over the resonance.

III. EXPERIMENTAL SEQUENCE

We load atoms into the optical tweezers from a magneto-optical trap around the PC. Operating in the collisional blockade regime [7], we monitor the fluorescence from each of the tweezers with our detector [Excelitas SPCM-AQRH-14-FC] and distinguish between having zero and one atom in each tweezer with fidelity of > 99 %. Every repetition of the experiment begins by triggering on the successful loading of both atoms (Fig. S4), followed by a 20 ms period of polarization gradient cooling to bring the atom's temperature down from 50 μK after loading to 15 μK.

The atoms are transported to the final positions on the PC by steering the individual galvanometer mirrors. Given that our cavity mode is 500 nm wide and 4 μm long, accurate positioning of the traps relative to the mode is crucial for the experiment. The position of the PC on the fiber tip can drift at a rate of ~ 100 nm/hour relative to the microscope objective. To correct for this drift, we pause the experiment every 20 minutes and acquire confocal images of the PC at different focal planes. The images are processed to determine the new position of the PC in three dimensions. In addition, every few days, we calibrate the atomic coupling strengths versus position and reposition the atoms such that they have equal coupling strength.

To take the reflection spectra, we probe the cavity with light resonant with $2 \rightarrow 3'$ transition while constantly depleting the $F = 1$ manifold with the individual repumpers. After acquiring the spectrum, we post-select the data for which an atom was loaded next to the cavity, which occurs with $\sim 70\%$ probability and is mainly limited by the initial temperature in the traps. We first prepare both atoms in the uncoupled ground state level $F = 1$ with a global beam resonant with the $5S_{1/2}$, $F = 2 \rightarrow 5P_{3/2}$, $F' = 1$ transition. Then we individually pump a single atom into the coupled ground state $F = 2$ with a beam resonant with the $5S_{1/2}$, $F = 1 \rightarrow 5P_{1/2}$, $F' = 2$ transition, co-propagating with the optical tweezers. After this selective pumping, we probe the cavity on resonance to determine the atom's presence in a single shot (Fig. 1d, main text). Repeating this procedure for the other atom allows us to select for data where one, the other, or both atoms are present. Once the experiment at the PC is finished, the tweezers are transported back to the original loading positions. The sequence is outlined in Fig. S4.

The probe experiment taking place at the cavity typically takes 500 μs, much shorter than the lifetime of atoms in the trap next to the PC of ~ 100 ms. Compared with the lifetime of 1.5 s away from the PC, the reduced lifetime next to the PC indicates additional heating mechanism, as previously observed by [8]. Understanding the sources of

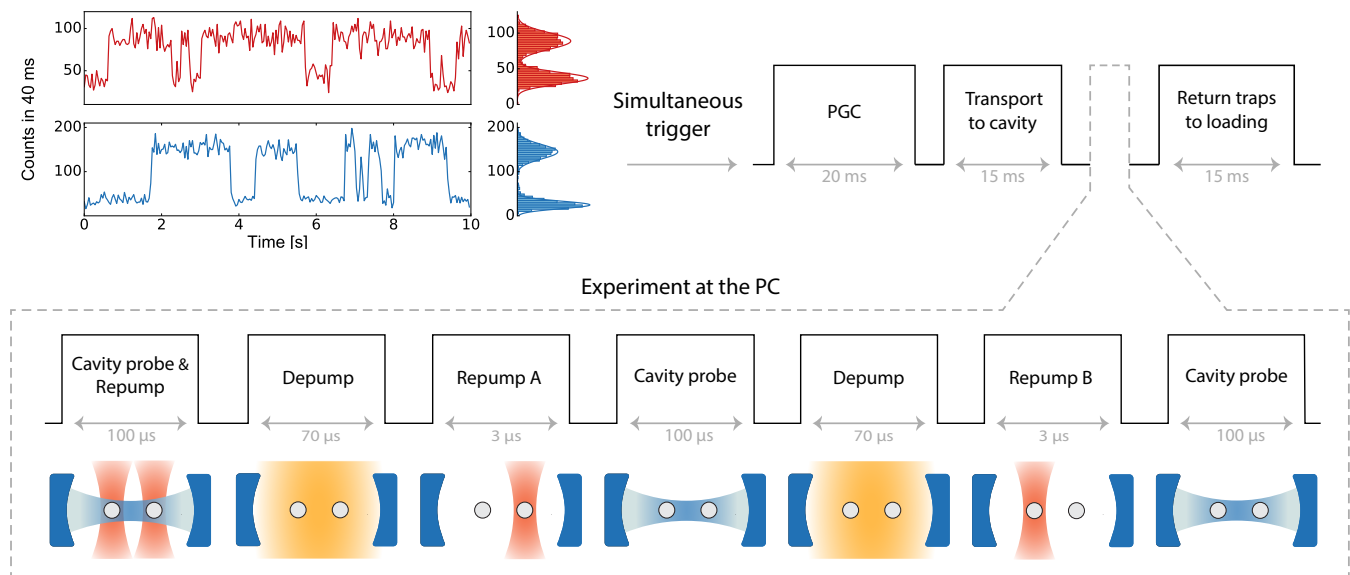extra heating and developing cooling techniques while next to the PC is a subject for future exploration.

FIG. S4: Experimental run is triggered upon rising edges of fluorescence counts from the atoms, followed by polarization gradient cooling (PGC). The sequence when the atoms are loaded next to the PC is depicted below, indicating which beams are global and which are local. The individual repumping beams are tuned to the $5S_{1/2}$, $F = 1 \rightarrow 5P_{1/2}$, $F' = 2$ transition, the global depumping beam to the $5S_{1/2}$, $F = 2 \rightarrow 5P_{3/2}$, $F' = 1$ transition. The data for spectra is taken from the first probe phase, while the second and third probe phases are used for individual atom post-selection.

IV. INDIVIDUAL TUNING OF THE ATOMIC RESONANCES

The independent optical tweezer paths in our setup allow for individual manipulation of the internal atomic states. In this work, we change the relative atomic detuning δ_{12} through light shifts from the individual tweezers. This is done by modulating their intensities out of phase. Tuning the contrast of the modulation then shifts the atoms in and out of resonance with respect to each other. Note that we choose the modulation frequency $\Delta_{\mathrm{mod}} \approx 2\pi \times 5$ MHz, which is faster than the motional frequencies of the traps, thereby subjecting the two atoms to the same average trapping potential. The intensity modulation is generated using a Mach-Zehnder interferometer, with an acousto-optic modulator (AOM) driven at $\omega_{\mathrm{AOM}} \pm \Delta_{\mathrm{mod}}/2$ in each arm, where $\omega_{\mathrm{AOM}} = 2\pi \times 80$ MHz is the central frequency of the AOMs. The relative phase between the two tweezers can be tuned by sending one of the outputs of the interferometer through a delay line (~ 100 m) and fine tuning the relative drive frequency Δ_{mod} to match the path difference. The modulated optical signal is also used to trigger the probe light sent to the cavity. Calibrating the delay of the triggered probe pulse allows us to probe the atoms at their maximum/minimum light shifts. When operating with the traps out of phase, changing the contrast of this modulation changes the individual lightshift of each atom and is used to sweep the atom-atom detuning as depicted in Fig. S5.
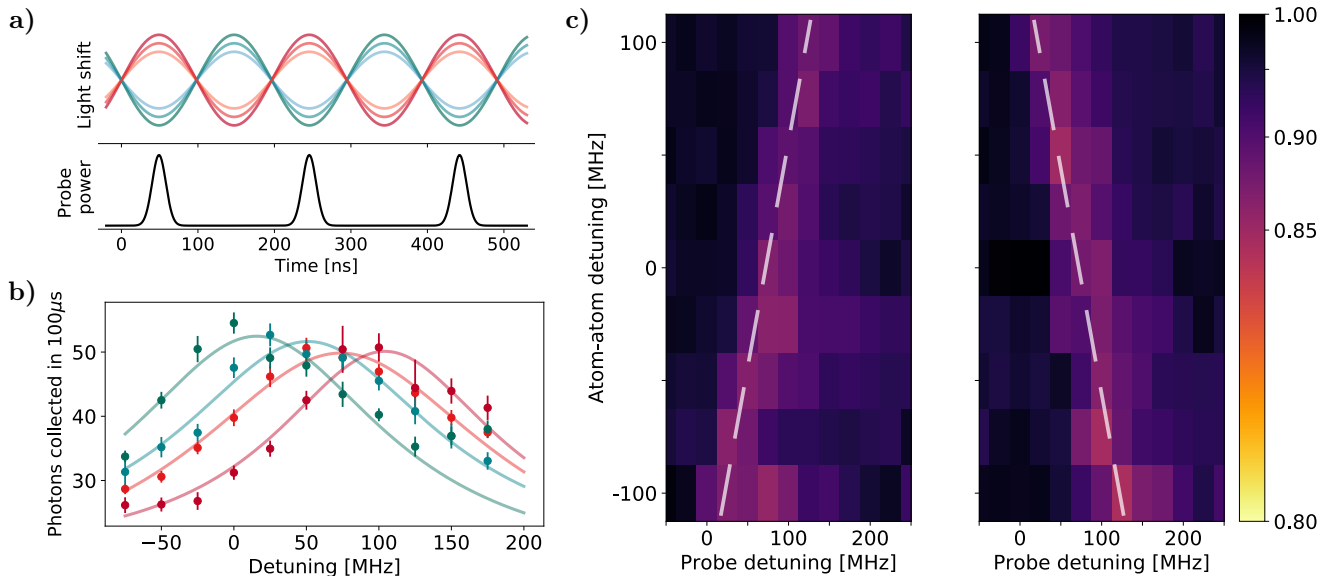
FIG. S5: **a)** Illustration of the instantaneous light shift experienced by each atom probed while modulating the individual tweezer intensity. **b)** Reflection spectra in the resonant regime at two different modulation contrasts (light/dark) for one atom (greens) and the other (reds) to show how the individual light shifting can be tuned simultaneously. **c)** Experimental data of reflectivity map over probe detuning and atom detuning in the dispersive regime showing light shift tuning.

V. THEORETICAL MODELS

To model the reflection spectra, we study the transitions between the $5S_{1/2}$, $F = 2$ ground state manifold, labeled $|g\rangle$, and the relevant excited states in $5P_{3/2}$ i.e. $F' = 1, 2, 3$, labeled $|e_i\rangle$, where $i = 1, 2, 3$. For the on-resonance measurements (FIGs. 1 and 2 in the main text), the cavity frequency ω_c is resonant with the $2 \to 3'$ transition. The cavity field decay rate ($\kappa = 2\pi \times 3.7$ GHz) is smaller than the hyperfine splitting between the $F = 1$ and $F = 2$ ($\Delta_{HF} = 2\pi \times 6.8$ GHz), so we neglect the cavity coupling to $F = 1$ manifold. Experimentally, we confirm this by noting that when the atom is in $F = 1$, the cavity reflectivity is the same as if there were no atom coupled to it.

A system consisting of a cavity and a multi-level atom is described by the Hamiltonian [10]:

$$H = \omega_c a^\dagger a + \sum_i \omega_i \sigma_i^\dagger \sigma_i + \sum_i g_i(a^\dagger \sigma_i + a \sigma_i^\dagger) \tag{1}$$

where $\sigma_i = |g\rangle \langle e_i|$ and a are the lowering operators for the atomic and cavity excitations respectively, g_i is the single-photon Rabi frequency between the cavity and the excited state $|e_i\rangle$, and ω_i is the resonance frequency between $|g\rangle$ and $|e_i\rangle$. Each excited state decays into free space at a rate γ, and cavity decays at a total rate κ, out of which κ_{wg} is into the collected waveguide mode.

To model the incoherent population decays from the atomic excited states and the cavity mode, we define the Lindblad jump operators $L_0 = \sqrt{\kappa}a$ and $L_i = \sqrt{\gamma}\sigma_i$. We use individual decay operators L_i instead of the cumulative decay operator $\sum_i L_i$ because $\gamma = 2\pi \times 6$ MHz is much smaller than the hyperfine splittings in the excited states of $2\pi \times \{267, 157\}$ MHz, so we can neglect the interference between the spontaneously emitted photons. We confirm this by numerically modelling and comparing both cases.

The system dynamics can be described with Heisenberg-Langevin equations of the form

$$\dot{A} = i[H, A] + \sum_i \left(L_i^\dagger A L_i - \frac{1}{2}(A L_i^\dagger L_i + L_i^\dagger L_i A)\right) \tag{2}$$

where $A \in \{a, \sigma_i\}$. After solving for a, the reflectivity can be obtained from the input-output relation:

$$a_{out} + a_{in} = \sqrt{\kappa_{wg}}a \tag{3}$$

$$r = \frac{a_{out}}{a_{in}} = \sqrt{\kappa_{wg}}\frac{a}{a_{in}} - 1 \tag{4}$$

The resulting system of equations reads:

$$\dot{a} = -i\omega_c a - i\sum_j g_j\sigma_j - \frac{\kappa}{2}a + \sqrt{\kappa_{wg}}a_{in} \tag{5}$$

$$\dot{\sigma}_i = -i\omega_i\sigma_i + ia\sum_j g_j\Big(|e_j\rangle\langle e_i| - \delta_{i,j}|g\rangle\langle g|\Big) - \frac{\gamma}{2}\sigma_i \tag{6}$$

We are interested in the frequency response of the reflection to a weak drive of frequency ω. Since the steady-state population in $|e_i\rangle$ is negligible in this weak excitation limit, we can substitute $|e_j\rangle\langle e_i| - \delta_{i,j}|g\rangle\langle g| \approx -1$. Solving these equations, we obtain the reflectivity

$$r = \kappa_{wg}\left(\frac{\kappa}{2} - i\delta_c + \sum_i \frac{g_i^2}{\gamma/2 - i\delta_i}\right)^{-1} - 1, \tag{7}$$

where $\delta_c = \omega - \omega_c$ and $\delta_i = \omega - \omega_i$. The expression has the same format as the one for multiple emitters coupled to the same cavity mode [11] and can be extended by modifying the sum to include multiple emitters. The cooperativity associated with the i-th transition is $C_i = 4g_i^2/\kappa\gamma$. The reflection spectra are measured as $|r(\omega)|^2$.

Atomic motion in the cavity mode

Nanophotonic structures confine photons to sub-wavelength mode volumes. The longitudinal confinement is a ~ 4 μm long gaussian envelope, and the transverse confinement is given by the evanescent field of decay with the characteristic length of $z_0 = 120$ nm [12]. Moreover, the mode intensity is longitudinally modulated with the lattice constant of $a = 290$ nm. Due to these spatial variations, an atom in motion will be subjected to a fluctuating coupling strength.
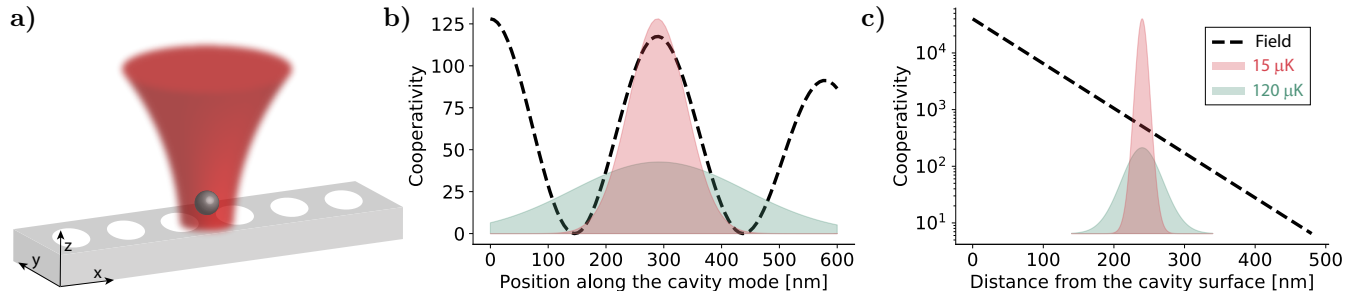

FIG. S6: **a)** Illustration of an atom trapped in a tweezer above the photonic crystal and definition of axes. **b)** Cooperativity variation in the longitudinal (x-axis) direction. The green and red dashed lines correspond to the atomic spatial width at 120 μK and 15 μK, respectively. **c)** Cooperativity variation and atomic spatial widths in the z direction.

The variation of the atomic position depends on its temperature and confinement length scale. Given the motional radial frequency measured to be $2\pi \times 115$ kHz, we obtain the size of of the atomic spatial width of 50 nm in the radial direction of the tweezer at 15 μK (the temperature reached after polarization gradient cooling). As the atoms are transported to the cavity, the trapping potential gains additional axial confinement from the reflection of the tweezer off of the structure [12]. The process of potential distortion from a gaussian beam to a standing wave can introduce heating to the atom. From separate measurements of the coherence times between two magnetic sublevels in the ground state at varying tweezer depths similar to [13], we estimate the upper bound for our temperature at the cavity to be 120 μK, corresponding to a spatial width of 150 nm in the radial direction of the tweezer.

The standing wave formed in the axial direction results in a higher axial frequency of $2\pi \times 550$ kHz. This tight confinement is crucial for the operation since the evanescent field decays sharply in the axial direction. Fig. S6 shows the variation of the cavity mode in the x- and z- directions, overlapped with our estimates of the {lower, upper} bound on spatial width at {15, 120} μK, corresponding to the axial widths of {12, 30} nm.

To account for the cavity field sampling, we model the cooperativity C, which is proportional to the field intensity I, to vary in the two directions as

$$C(x, z) = C_0 \cos^2\left(\frac{\pi x}{a}\right)e^{-2z/z_0} \tag{8}$$

where $a = 290$ nm, $z_0 = 120$ nm, and C_0 is the cooperativity the atom would experience in the absence of motion at its center position $(x, z) = (0, 0)$. Note that we have neglected the slowly-varing envelope in the direction along the standing wave with the characteristic mode length of 4 μm as well as the variation in the y direction.

Cooperativity estimation

To model our experimental reflection spectrum (e.g. Fig. 1d, main text) and extract an estimate for the associated cooperativity, we combine the expression for reflectivity in Eq.(7) with the spatial dependence of the cooperativity in Eq.(8). To produce a spectrum, we sample atomic positions in the x and z directions (as defined in Fig. S6a) from normal distributions with standard deviations w_x and w_z respectively and generate a reflectivity averaged over multiple values of the resulting cooperativities. The fit parameters consist of w_x, w_z, and the cooperativity amplitude $C_{0,i}$ in Eq.(8) associated with transition to each excited state $|e_i\rangle$.
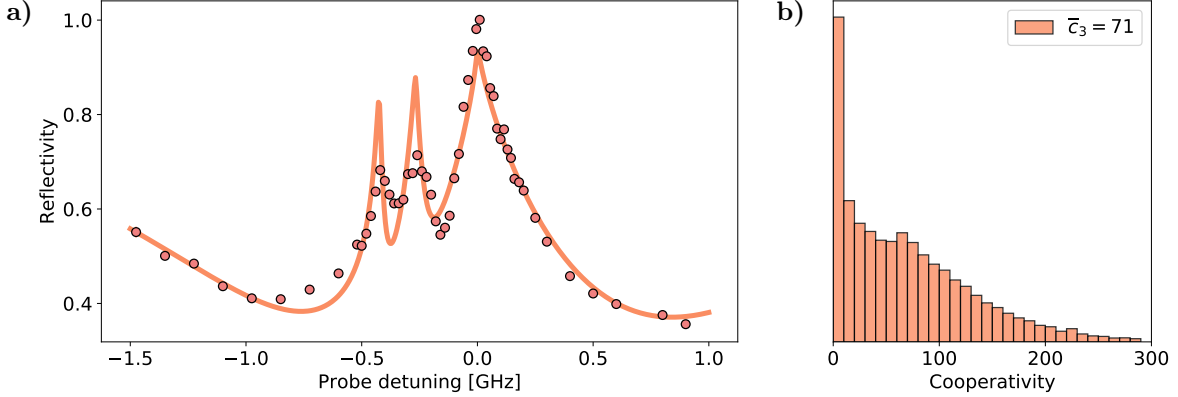

FIG. S7: **a)** Theoretical model for the single-atom reflection spectrum at the mode maximum overlapped with experimental data. **b)** Associated cooperativity distribution with the mean of 71(4) and standard deviation of 66(4).

The best fit (Fig. S7a) for the data according to this model yields $w_x = 190$ nm, $w_z = 33$ nm. The cooperativity associated with the 3' line of interest is $C_{0,i=3} = 128(6)$ in the absence of motion. The histogram of the cooperativity distribution associated with the spectrum is shown in Fig. S7b, yielding the mean of $\langle C_{i=3}\rangle = 71(4)$, and the standard deviation of 66(4). The uncertainties are determined by bootstrapping.

The value of C_0 extracted is consistent with our independent estimate of the field strength at the surface of the PC of $2g_{max} \approx 2\pi \times 15$ GHz which evanescently decays down to $2g_0 \approx 2\pi \times 1.7$ GHz at 260 nm away from the PC. The single-photon Rabi frequency at the surface $2g_{max}$ (corresponding to the maximum cooperativity of $C_{max} \approx 40,000$) is calculated from the single-photon electric field of $E_{max} \approx 2$ kV/cm, estimated for the mode volume $V_{mode} = 0.4\lambda^3$ [12]. The biggest deviation from the model occurs in the height of the 1' and 2' lines. Some of the effects neglected in this model include decays to $F = 1$ ground state and repumping from it (which could explain the reduced heights), the motion in the y direction, heating during probing, and trap pointing uncertainty.

The two-atom spectrum (FIG 2, main text) is taken with atoms placed 1 μm away from the mode center. We now focus on the 3' line, which is also the transition we use in the dispersive regime. The fit to the single-atom reflectivity at this position is shown in Fig. S8. The spatial widths $w_x = 190$ nm, $w_z = 33$ nm, are the same as those in Fig. S7, whereas $C_{0,i=3} = 56(3)$, corresponding to the mean single-atom cooperativity of $\langle C_{i=3}\rangle = 31(2)$ and the standard deviation of 28(2), averaged over two atoms. The reduction of the mean cooperativity is expected from the mode profile shown in Fig. 2c in the main text. The two-atom reflection spectrum is generated based on both single-atom spectra with no additional parameters.
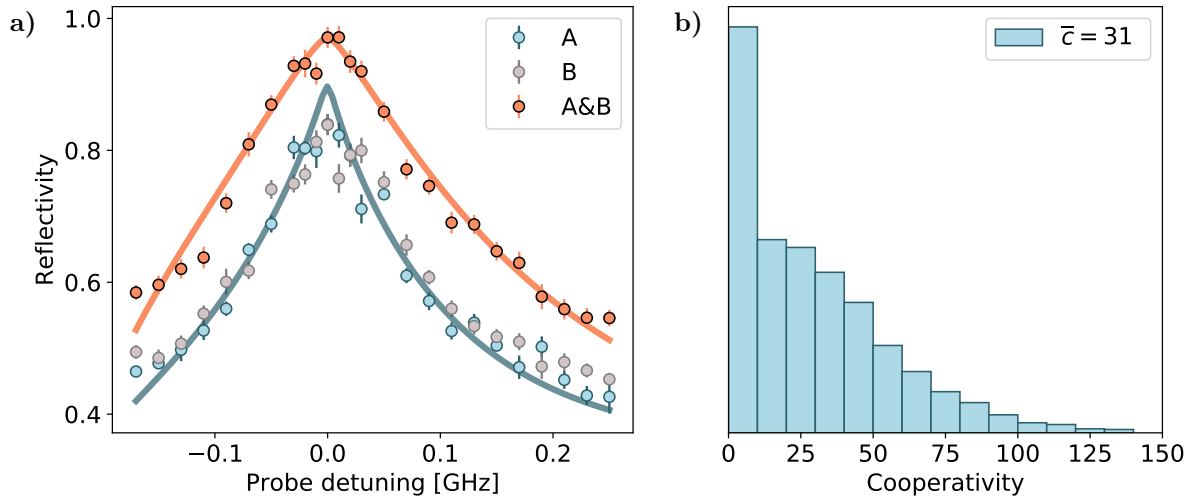
FIG. S8: **a)** Theoretical model for the single-atom reflection spectrum 1 μm away from the mode center (blue) and for the two-atom reflection spectrum (red) generated using the same cooperativity distribution. **b)** Distribution of single-atom cooperativity for the $2 \to 3'$ transition.

The spectra in the dispersive regime taken with nonzero light shifts (Fig. 3b, 4, main text) are analyzed with the same model. In addition, we take into account the effect of fluctuating light shift $\delta_{A,B}$ due to atomic motion. We extract $J = 2\pi \times 25(4)$ MHz at $\Delta = 2\kappa$, consistent with our cooperativity estimate for the resonant regime.

[1] T. G. Tiecke, K. P. Nayak, J. D. Thompson, T. Peyronel, N. P. de Leon, V. Vuletić, and M. D. Lukin, "Efficient fiber-optical interface for nanophotonic devices," *Optica* **2**, 70-75 (2015).

[2] E. R. I. Abraham and E. A. Cornell, "Teflon feedthrough for coupling optical fibers into ultrahigh vacuum systems," *Appl. Opt.* **37**, 1762-1763 (1998).

[3] S. Gröblacher, J. T. Hill, A. H. Safavi-Naeini, J. Chan, and O. Painter, "Highly efficient coupling from an optical fiber to a nanoscale silicon optomechanical cavity," *Appl. Phys. Lett.* **103**, 181104 (2013).

[4] J. Chan, M. Eichenfield, R. Camacho, and O. Painter, "Optical and mechanical design of a "zipper" photonic crystal optomechanical cavity," *Opt. Express* **17** , 3802-3817 (2009).

[5] T. G. Tiecke, J. D. Thompson, N. P. de Leon, L. R. Liu, V. Vuletić and M. D. Lukin, "Nanophotonic quantum phase switch with a single atom," *Nature* **508**, 241-244 (2014).

[6] E. D. Black, "An introduction to Pound-Drever-Hall laser frequency stabilization," *Am. J. Phys.* **69**, 79 (2001).

[7] N. Schlosser, G. Reymond, and P. Grangier, "Collisional Blockade in Microscopic Optical Dipole Traps," *Phys. Rev. Lett.* **89**, 023005 (2002).

[8] D. Hümmer, P. Schneeweiss, A. Rauschenbeutel, and O. Romero-Isart, "Heating in Nanophotonic Traps for Cold Atoms," *Phys. Rev. X* **9**, 041034 (2019).

[9] J. D. Thompson, T. G. Tiecke, A. S. Zibrov, V. Vuletić, and M. D. Lukin, "Coherence and Raman Sideband Cooling of a Single Atom in an Optical Tweezer," *Phys. Rev. Lett.* **110**, 133001 (2013).

[10] K. M. Birnbaum, A. S. Parkins, and H. J. Kimble, "Cavity QED with multiple hyperfine levels", *Phys. Rev. A* **74**, 063802, (2006).

[11] R. E. Evans, M. K. Bhaskar, D. D. Sukachev, C. T. Nguyen, A. Sipahigil, M. J. Burek, B. Machielse, G. H. Zhang, A. S. Zibrov, E. Bielejec, H. Park, M. Lončar, M. D. Lukin, "Photon-mediated interactions between quantum emitters in a diamond nanocavity," *Science* **362**, 662-665 (2018).

[12] J. D. Thompson, T. G. Tiecke, N. P. de Leon, J. Feist, A. V. Akimov, M. Gullans, A. S. Zibrov, V. Vuletić, and M. D. Lukin, "Coupling a single trapped atom to a nanoscale optical cavity," *Science* **340**, 1202-1205 (2013).

[13] Kuhr, S. and Alt, W. and Schrader, D. and Dotsenko, I. and Miroshnychenko, Y. and Rauschenbeutel, A. and Meschede, D., "Analysis of dephasing mechanisms in a standing-wave dipole trap," *Phys. Rev. A* **72**, 023406 (2005).